Hindawi
Shock and Vibration
Volume 2019, Article ID 5389732, 18 pages
https://doi.org/10.1155/2019/5389732

Research Article

Dynamic Response Analysis of Planar Multilink Mechanism considering Wear in Clearances

Shuai Jiang, Xiulong Chen, and Yu Deng

College of Mechanical and Electronic Engineering, Shandong University of Science and Technology, Qingdao 266590, China

Correspondence should be addressed to Xiulong Chen; cxldy99@163.com

Received 21 May 2019; Revised 23 July 2019; Accepted 6 August 2019; Published 28 August 2019

Academic Editor: Athanasios Chasalevris

Clearance wear is one of the factors that affects dynamics for mechanical systems. A numerical methodology suitable for modeling and calculation of wear at multiple revolute clearance pairs in the field of the planar multilink mechanism is proposed. In this paper, the 2-DOF nine-bar mechanism considering two revolute clearance joints is regarded as the study object. Normal contact force and friction force models of revolute clearance joints used Lankarani–Nikravesh (L-N) and LuGre models, respectively. The iterative wear prediction process based upon Archard's model has been applied to calculate wear characteristics. The wear prediction procedure is integrated with multibody dynamics, wear depths at revolute clearance joints are calculated, and the surface of shaft and bearing is reconstructed twice. The dynamic responses of mechanism considering two nonregular revolute clearances caused by wear are studied in depth. The nonlinear characteristics of the mechanism after wear are studied by the phase diagram and Poincaré map. Influences of different initial constant clearance values and different driving speeds on wear of two revolute joints are also researched. The results show that it is necessary to consider the factor of irregular clearances caused by wear in analysis of dynamics of precision mechanisms. Initial constant clearance values and driving speeds have some influence on wear phenomenon. This research provides a theoretical basis for studying dynamics of the planar multilink mechanism considering wear in multiple clearances.

1. Introduction

In the actual mechanical mechanism, the clearance of the motion pair is unavoidable [1–4]. With the development of precision mechanical engineering, it is increasingly necessary to accurately predict the wear phenomenon of mechanical system. In the process of contact movement of pair elements, the surface material of pair element will be constantly losing, which will increase the clearance value at motion pair. And the dynamic responses of the mechanism will be changed accordingly [5–7]. In particular, wear prediction of the mechanism system containing multiple clearance joints is one of the crucial questions to be settled urgently. Therefore, it is of great practical value to study dynamic wear phenomena of motion pairs.

In the last few years, many scholars have done plenty of researches on dynamics behavior for mechanical systems considering constant clearances. However, there are few studies on dynamic responses for multibody mechanical systems considering nonregular clearances. Tan et al. [8] explored dynamics response for the slider crank mechanism containing clearances. And the dynamics model was built through combining the Newton–Euler method and improved the Coulomb friction force model together, and the Baumgarte stabilization approach was used to enhance numerical stability. Wang et al. [9] proposed a nonpenetration methodology for frictional contact analysis for modeling clearance of the planar crank-slider mechanism. Chen et al. [10] conducted the dynamic simulations of the crank-slider mechanism considering clearance, flexibility, and friction by using ADAMS. Influences of link flexibility and clearance value on dynamic response were researched. Wang et al. [11] discussed nonlinear dynamics for the flexible crank-slider mechanism considering clearance at one revolute pair and modeled flexible dynamic equations by utilizing ANCF. Zheng et al. [12] established a flexible dynamics model for high-precision press mechanism considering clearance and lubrication. Effects of clearance size,

blanking force, and input crank speed on dynamics behavior of the multilink mechanism have been also studied. Muvengei et al. [13] studied nine motion modes of two rotating clearance pairs and the influence of clearances on the dynamic response for the crank-slider mechanism. Normal force and frictional force at revolute clearances have been, respectively, modeled by the L-N contact force model and LuGre model. Flores et al. [14] presented a method to discuss influence of the clearance value and friction coefficient on dynamic performance for the planar four-bar mechanism containing revolute clearance joints. Through utilizing Poincaré maps, periodic responses and chaotic responses for the four-bar mechanism were both observed. Chen et al. [15] developed the nonlinear dynamic model for 2-DOF nine-bar mechanism containing clearance and flexibility rods through using the Lagrange equation and FEM. Yaqubi et al. [16] analyzed dynamics behavior of a crank-slider mechanism containing clearance pairs and investigated nonlinear dynamic by Poincaré maps and bifurcation diagrams. Influences of the friction on dynamic responses and nonlinear characteristics are also discussed. Muvengei et al. [17] discussed dynamic response of the crank-slider mechanism existing stick-slip friction at revolute clearance pairs. And the LuGre model was presented to express stick-slip friction at revolute clearance pairs.

As is well known, existence of clearance at kinematic pair causes wear, which will directly reduce the life of mechanism. However, the research studies on wear of planar mechanisms are mainly concentrated upon simple planar mechanisms containing single revolute clearance pair and mainly concentrated on wear depth and surface reconstruction. Few studies have been done on dynamic response for the planar complex mechanism considering multiple clearances after many times wear by combining the L-N model with the LuGre friction model. Flores [18] developed a method for researching and quantifying wear at revolute pair including clearance. The simple planar four-bar mechanism is utilized to perform numerical simulations. Li et al. [19] analyzed wear phenomenon at two revolute clearance pairs in the crank-slider mechanism through coupling dynamic with tribology. And the effect of diverse constant clearance sizes on wear depth was also studied. Bai et al. [20] investigated wear prediction at revolute pair for four-bar mechanism by using a computational method. A novel hybrid contact force and a modified Coulomb friction model were, respectively, used as normal contact and friction models. And it discussed the dynamics performance and wear phenomenon on the four-bar mechanism considering single revolute clearance joint. Zhao et al. [21] put forward a numerical methodology to predict the wear of revolute pairs considering clearances for the flexible planar crank-slider mechanism. The normal contact force of the clearance joint used the L-N model, and friction force adopted the LuGre model. Archard's model was applied to forecast wear, and wear depth was also calculated. Mukras et al. [22] put forward a procedure to discuss the dynamic of the crank-slider mechanism. Wear prediction at revolute clearance pair is presented based upon Archard's model. The procedure was validated by comparing wear prediction with the wear experiment. Bai et al. [23] researched dynamic response and wear phenomenon at single revolute joint of the four-bar mechanism by using a computational method. An integrated method of dynamic response analysis and wear analysis was proposed. Xiang et al. [24] proposed and discussed the comprehensive method to predict wear in the planar crank-slider mechanism containing clearance joints. The wear process has been integrated into a differential equation to perform coupling iteration analysis of dynamics response and wear prediction. Wang et al. [25] predicted the effect of spherical clearance caused by the wear on dynamic behavior for spatial four-bar mechanism based upon Archard's model.

Through above description, in the research field of planar multibody dynamics system considering clearance wear, previous literatures mainly concentrated upon study of the simple mechanism (such as the crank-slider mechanism and four-bar mechanism) considering single revolute clearance joint and the research of wear depth and surface reconstruction of the shaft and bearing after wear. And few studies have been done on dynamic responses and nonlinear dynamic characteristics for the planar multilink mechanism containing multiple revolute clearances by adopting the LuGre model after many times wear. In this paper, the dynamic model of the multilink mechanism considering wear at multiple clearance joints by using the LuGre model is developed, and dynamic responses of the multilink mechanism containing multiple clearance joints after many times wear are studied systematically and in detail. The nonlinear characteristics of the mechanism after wear are studied by the phase diagram and Poincaré map. The influences of different factors on wear at multiple clearance joints are researched.

This paper is organized as followed: In Section 1, the clearance model of the revolute joint is established. In Section 2, the dynamic model of 2-DOF nine-bar mechanism considering two revolute clearance joints is established. In Section 3, based upon Archard's model, the wear model of the clearance of the rotating pair is established. In Section 4, wear depth of the two revolute clearance joints is forecasted, and the surface of shaft and bearing is reconstructed twice. The dynamic responses after twice wear of 2-DOF nine-bar mechanism considering constant clearance and nonregular clearance caused by wear are both discussed, which include kinematic characteristics of the slider, shaft center trajectories, the contact forces at clearance joints, and the input driving torques of cranks. The nonlinear characteristics of the mechanism after wear are studied by the phase diagram and Poincaré map. The influences of different initial constant clearance sizes and different driving speeds on wear are researched. Finally, main conclusions are drawn.

2. Establishment of Clearance Model

2.1. Kinematic Model of Revolute Clearance Joint. As illustrated in Figure 1, it is shown that bearing i and shaft j are connected via a revolute clearance pair. R_i and R_j, respectively, represent the radius of bearing and shaft. Clearance size is defined as $c = R_i - R_j$. Global coordinate

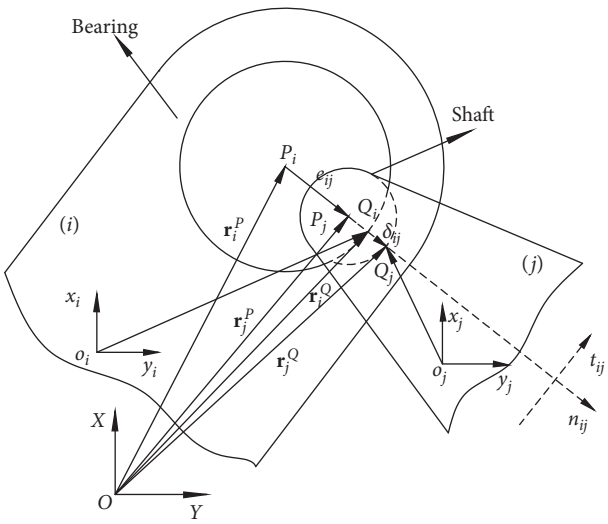

Figure 1: Revolute clearance model.

system is XOY. Local coordinate systems of the bearing and shaft are $x_io_iy_i$ and $x_jo_jy_j$, respectively. P_i and P_j are the rotating center of bearing and the shaft, and the position vector in the fixed coordinate system is $\mathbf{r}_i^P$ and $\mathbf{r}_j^P$.

Eccentricity vector and eccentricity between bearing and shaft are

$$\begin{aligned} \mathbf{e}_{ij} &= \mathbf{r}_j^P - \mathbf{r}_i^P, \\ e_{ij} &= \sqrt{\mathbf{e}_{ij}^T \mathbf{e}_{ij}}. \end{aligned} \tag{1}$$

Unit normal vector could be written as

$$\mathbf{n}_{ij} = \frac{\mathbf{e}_{ij}}{e_{ij}}. \tag{2}$$

While shaft and bearing impact with each other, penetration depth can be expressed as

$$\delta_{ij} = e_{ij} - c. \tag{3}$$

When $\delta_{ij} < 0$, bearing and shaft are in the free flight mode. When $\delta_{ij} = 0$, bearing and shaft are in the continuous contact mode. When $\delta_{ij} > 0$, bearing and shaft are in the impact mode.

Contact point Q_i and Q_j in the global coordinate system could be written as

$$\mathbf{r}_k^Q = \mathbf{r}_k^P + R_k \mathbf{n}_{ij}, \quad k = i,\ j. \tag{4}$$

Velocity of contact point Q_i and Q_j is

$$\dot{\mathbf{r}}_k^Q = \dot{\mathbf{r}}_k^P + R_k \dot{\mathbf{n}}_{ij}, \quad k = i, j. \tag{5}$$

Relative velocities in the normal direction and tangential direction could be given by

$$\begin{cases} v_n = \left(\dot{\mathbf{r}}_j^Q - \dot{\mathbf{r}}_i^Q\right)^T \mathbf{n}_{ij}, \\ v_t = \left(\dot{\mathbf{r}}_j^Q - \dot{\mathbf{r}}_i^Q\right)^T \mathbf{t}_{ij}. \end{cases} \tag{6}$$

2.2. The Normal Force Model. The Lankarani–Nikravesh contact force model is more suitable for general mechanical contact with the high coefficient of restitution, particularly while energy dissipation is relatively few [13, 22]. The L-N model is well conformity to experimental results. And it is straightforward for the numerical integration algorithm [8, 14, 21]. Therefore, the L-N model has been applied in this paper:

$$F_n = K\delta_{ij}^n + D\dot{\delta}_{ij}, \tag{7}$$

where Krepresents the stiffness parameter; D represents the damping coefficient; n represents a constant decided by the material property of contact surface; for metal surface, $n = 1.5$; and $\dot{\delta}_{ij}$ is the penetration velocity.

Stiffness parameter K can be given by

$$K = \frac{4}{3\pi\left(\sigma_i + \sigma_j\right)}\left(\frac{R_iR_j}{R_i + R_j}\right)^{1/2}, \tag{8}$$

where $\sigma_i = (1 - \nu_i^2)/(\pi E_i)$ and $\sigma_j = (1 - \nu_j^2)/(\pi E_j)$, in which ν_i and ν_j represent Poisson's ratio of the bearing and shaft, respectively. E_i and E_j represent the elastic modulus of bearing and shaft. Radius is negative for concave surfaces and positive for the convex surface.

Damping coefficient D could be expressed by

$$D = \frac{3K\left(1 - c_e^2\right)\delta_{ij}^n}{4\dot{\delta}_{ij}^{(-)}}, \tag{9}$$

where c_e means the restitution coefficient; $\dot{\delta}_{ij}^{(-)}$ is the initial impact velocity; if $\delta_{ij}(t_n)\delta_{ij}(t_{n+1}) \le 0$, $\delta_{ij}(t_n) < 0$ and $\delta_{ij}(t_{n+1}) > 0$; contact occurs between two discrete times of t_n and t_{n+1}; and penetration velocity at t_{n+1} represents the initial impact velocity $\dot{\delta}_{ij}^{(-)}$.

2.3. The Tangential Force Model of Revolute Clearance. LuGre model was presented by the Canudas de Wit et al. It can capture the change of friction force with the slip speed. Therefore, it is suitable for the study of stick-slip motion. The LuGre model can also be utilized to capture the Stribeck phenomenon [26]. According to classical definition of friction, the friction force could be expressed as follows [17, 21]:

$$F_t = \mu F_n. \tag{10}$$

The instantaneous coefficient of friction μ is viewed to vary as a function of tangential velocity and an average bristle deflection z, and we can get the following [10]:

$$\mu = \sigma_0 z + \sigma_1 \dot{z} + \sigma_2 v, \tag{11}$$

where σ_0 represents the bristle stiffness, σ_1 represents the microscopic damping coefficient, σ_2 represents the viscous friction coefficient, and v is the tangential velocity.

Evolution differential equation of average bristle deflection [13, 27] could be given by

$$\dot{z} = v - \frac{\sigma_0|v|}{\mu_k + (\mu_s - \mu_k)e^{-|v/v_s|\gamma}} z, \tag{12}$$

where μ_k represents the kinetic friction coefficient that is a measure of Coulomb friction force, μ_s represents the static friction coefficient which is a measure of stiction force, γ represents the gradient of friction decay, and v_s represents the stribeck velocity.

Substituting equation (12) into equation (11), then

$$\mu = \sigma_0 z\left(1 - \frac{\sigma_0|v|}{\mu_k + (\mu_s - \mu_k)e^{-|v/v_s|\gamma}}\right) + (\sigma_1 + \sigma_2)v. \tag{13}$$

In this paper, choice of z was based upon following assumptions [17]: because simulations at the steady-state condition are required, average bristle deflection z was supposed to be a constant for a particular value of relative tangential velocity of components. Hence, at steady state, z could be given by

$$\begin{cases} \dot{z} = v - \dfrac{\sigma_0|v|}{\mu_k + (\mu_s - \mu_k)e^{-|v/v_s|\gamma}} z = 0, \\ z = \dfrac{v}{|v|} \cdot \dfrac{\mu_k + (\mu_s - \mu_k)e^{-|v/v_s|\gamma}}{\sigma_0}. \end{cases} \tag{14}$$

2.4. Force Analysis of the Revolute Clearance. The force and moment acting on the centroid of bearing i are written as

$$\begin{aligned} F_{ij} &= F_n\mathbf{n} + F_t\mathbf{t} = \left[F_{ij}^x F_{ij}^y\right]^T, \\ M_{ij} &= -\left(y_i^Q - y_i\right)F_{ij}^x + \left(x_i^Q - x_i\right)F_{ij}^y. \end{aligned} \tag{15}$$

The force and moment acting on the centroid of shaft j are expressed as

$$\begin{aligned} F_{ji} &= -F_{ji}, \\ M_{ji} &= -\left(y_j^Q - y_j\right)F_{ji}^x + \left(x_j^Q - x_j\right)F_{ji}^y. \end{aligned} \tag{16}$$

3. Dynamic Model of 2-DOF Nine-Bar Mechanism considering Revolute Clearances

A 2-DOF nine-bar mechanism is taken as a research object, which consists of the frame, crank 1, rod 2, rod 3, crank 4, rod 6, triangular panel 7, rod 8, and slider 9. Rod 5 is frame [15]. Two cranks are driven by the motors, and the DOF of mechanism is 2.

Crank 1 and rod 2 are connected through a revolute clearance pair A, and rod 3 and crank 4 are connected through a revolute clearance pair B. Crank 1 and crank 4 are driven by motors directly. Therefore, clearance at joint A and joint B could better reflect influence of revolute clearances on dynamics responses. Structure diagram of 2-DOF nine-bar mechanism considering two revolute clearance joints is displayed in Figure 2.

Local coordinate systems are built on centroid of each component. Generalized coordinates of the each member can be given by

$$\mathbf{q}_i = \left(x_i \;\; y_i \;\; \theta_i\right)^T, \quad i = 1, 2, 3, 4, 6, 7, 8, 9, \tag{17}$$

where x_i and y_i are the coordinates of centroid for component i in the global coordinate system and θ_i represents the angle for component i in the global coordinate system. Velocity and acceleration of generalized coordinates could be expressed as

$$\begin{cases} \dot{\mathbf{q}}_i = \left(\dot{x}_i \dot{y}_i \dot{\theta}_i\right)^T, \\ \ddot{\mathbf{q}}_i = \left(\ddot{x}_i \ddot{y}_i \ddot{\theta}_i\right)^T, \quad i = 1, 2, 3, 4, 6, 7, 8, 9. \end{cases} \tag{18}$$

When the clearance exists in the revolute pair, the constraints at the revolute pair are lost; that is, the corresponding constraints in the X and Y directions are deleted. Compared with the constraint equation without clearances, the number of constraint equations of the 2-DOF nine-bar mechanism containing revolute clearance joint A and revolute clearance joint B is reduced to 20, and the constraint equations considering revolute clearance joint A and revolute clearance joint B could be expressed as

$$\mathbf{\Phi}(\mathbf{q}, t) = \begin{pmatrix} x_1 - L_{s1}\cos\theta_1 \\ y_1 - L_{s1}\sin\theta_1 \\ x_4 - L_{s4}\cos\theta_4 - L_5 \\ y_4 - L_{s4}\sin\theta_4 \\ x_7 + L_{s72}\cos(\theta_7 - \beta_1) - x_2 - L_{s2}\cos\theta_2 \\ y_7 + L_{s72}\sin(\theta_7 - \beta_1) - y_2 - L_{s2}\sin\theta_2 \\ x_7 + L_{s72}\cos(\theta_7 - \beta_1) - x_3 - L_{s3}\cos\theta_3 \\ y_7 + L_{s72}\sin(\theta_7 - \beta_1) - y_3 - L_{s3}\sin\theta_3 \\ x_6 - L_{s6}\cos\theta_6 + H_x \\ y_6 - L_{s6}\sin\theta_6 - H_y \\ x_7 - L_{s71}\cos(\theta_7 + \beta) - x_6 - L_{s6}\cos\theta_6 \\ y_7 - L_{s71}\sin(\theta_7 + \beta) - y_6 - L_{s6}\sin\theta_6 \\ x_7 + L_{s73}\cos(\theta_7 + \beta_{12} + w_{12}) - x_8 + L_{s8}\cos\theta_8 \\ y_7 + L_{s71}\sin(\theta_7 + \beta_{12} + w_{12}) - y_8 + L_{s8}\sin\theta_8 \\ x_9 + H_x - L_6\cos\theta_6 - L_{72}\cos(\theta_7 + \beta_{12}) - L_{s8}\cos\theta_8 \\ y_9 - H_y - L_6\sin\theta_6 - L_{72}\sin(\theta_7 + \beta_{12}) - L_{s8}\sin\theta_8 \\ y_9 - H_y \\ \theta_9 \\ \theta_1 - \omega_1 t - 60.28^\circ \\ \theta_4 - \omega_4 t + 52.86^\circ \end{pmatrix} = 0. \tag{19}$$

Taking the first derivative of equation (19) with respect to time, the velocities of constraint equations containing revolute clearance joint A and revolute clearance joint B could be written as

$$\mathbf{\Phi}_q\dot{\mathbf{q}} = -\mathbf{\Phi}_t \equiv \mathbf{v}, \tag{20}$$

where $\mathbf{\Phi}_q$ represents the Jacobian matrix of constraint equations, $\mathbf{\Phi}_q = \partial\mathbf{\Phi}/\partial\mathbf{q}$, and $\mathbf{\Phi}_t$ represents the derivative of constraint equation to time, $\mathbf{\Phi}_t = \partial\mathbf{\Phi}/\partial t$.

Taking the first derivative of equation (20) with respect to time, accelerations of constraint equations containing two revolute clearances could be written as

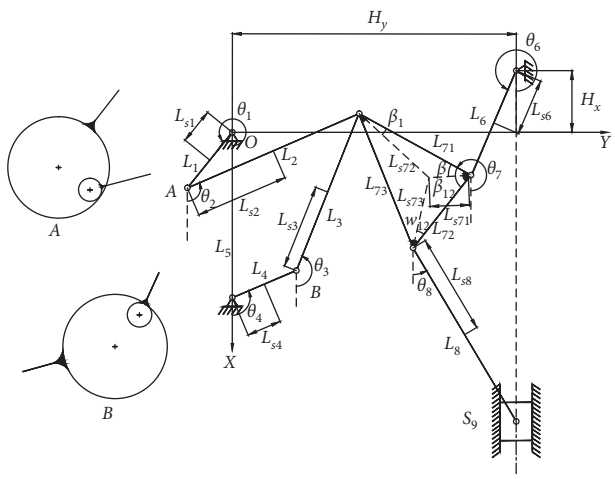

Figure 2: Structure diagram of 2-DOF nine-bar mechanism with revolute clearances.

$$\mathbf{\Phi}_q\ddot{\mathbf{q}} = -\left(\mathbf{\Phi}_q\dot{\mathbf{q}}\right)_q\dot{\mathbf{q}} - 2\mathbf{\Phi}_{qt}\dot{\mathbf{q}} - \mathbf{\Phi}_{tt} \equiv \boldsymbol{\gamma}. \tag{21}$$

Dynamics equations of the 2-DOF nine-bar mechanism considering revolute clearance joint A and revolute clearance joint B could be written as

$$\mathbf{M}\ddot{\mathbf{q}} + \mathbf{\Phi}_q^T\boldsymbol{\lambda} = \mathbf{F_g}, \tag{22}$$

where $\mathbf{M}$ represents the system mass matrix, $\boldsymbol{\lambda}$ represents the vector of Lagrange multiplier, and $\mathbf{F_g}$ represents the vector of generalized force vector.

Multibody dynamic equations containing revolute clearance joint A and revolute clearance joint B in the differential algebraic form could be formed by equations (21) and (22):

$$\begin{pmatrix} \mathbf{M} & \mathbf{\Phi}_q^T \\ \mathbf{\Phi}_q & 0 \end{pmatrix}\begin{pmatrix} \ddot{\mathbf{q}} \\ \boldsymbol{\lambda} \end{pmatrix} = \begin{pmatrix} \mathbf{F_g} \\ \boldsymbol{\gamma} \end{pmatrix}^T. \tag{23}$$

Equation (23) does not directly apply the displacement constraint and velocity constraint equations of the system, which bring about default of equations. At present, the most common and effective method is the default stability algorithm proposed by Baumgarte [8]. In this method, displacement constraints and velocity constraint are introduced into the acceleration constraints equation by feedback control theory so as to reduce the default of system. Therefore, it could be written as follows:

$$\begin{pmatrix} \mathbf{M} & \mathbf{\Phi}_q^T \\ \mathbf{\Phi}_q & 0 \end{pmatrix}\begin{pmatrix} \ddot{\mathbf{q}} \\ \boldsymbol{\lambda} \end{pmatrix} = \begin{pmatrix} \mathbf{F_g} \\ \boldsymbol{\gamma}' \end{pmatrix}^T, \tag{24}$$

where $\boldsymbol{\gamma}' = \boldsymbol{\gamma} - 2\alpha\dot{\mathbf{\Phi}} - \beta^2\mathbf{\Phi}$, α and β are correction parameters greater than 0, and $\dot{\mathbf{\Phi}} = d\mathbf{\Phi}/dt$.

Since equation of system (equation (24)) is complex, it is nearly impossible to be solved analytically. Therefore, in order to guarantee accuracy and efficiency, Runge–Kutta methodology has been used to solve equations through MATLAB.

4. Wear

4.1. Wear Modeling in Revolute Clearance Joint. In the multibody mechanical system, while two components of revolute pair are in contact with each other or in relative motion, the surface of the two components will be worn due to the contact force produced by the collision, which makes the surface no longer smooth. Therefore, it is very important to forecast the wear phenomenon at the revolute clearance pairs.

Archard's model connects wear volume with some physical and geometrical properties of sliding components, such as sliding distance, hardness, and applied load [18, 21]. Moreover, its construction is simple and it is most close to the adhesive wear mechanism, and Archard's model is validated by experimental results. Therefore, it is widely applied in wear prediction for the multibody mechanical system [5, 6, 24]. So, it could be written as

$$\frac{V}{s} = k\frac{F_n}{H}, \tag{25}$$

where V represents the wear volume, k represents the dimensionless wear coefficient, F_n represents the normal contact force, H represents the Brinell hardness of soft materials, and s is the sliding distance.

Contact form and geometric relationship of revolute pair considering clearance are shown in Figure 3. $e_{ij} = |P_iP_j|$ and $\overline{\beta}$ is the contact angle.

According to the cosine theorem, the contact angle can be expressed as

$$\overline{\beta} = \arccos\frac{e_{ij}^2 + R_i^2 - R_j^2}{2e_{ij}R_i}. \tag{26}$$

In ΔDP_iC,

$$|\mathrm{DC}| = R_i\sin(\pi - \overline{\beta}). \tag{27}$$

In fact, $\angle DP_jC$ is far bigger than the real because penetration depth δ_{ij} is far smaller than R_i and R_j. So the length of contact arc CE along the circumferential direction is equal approximately to |DC|; that is, $|\mathrm{DC}| \approx \mathrm{CE}$ [7].

Therefore, actual contact area A_a could be expressed as

$$A_a \approx |\mathrm{DC}| \cdot w, \tag{28}$$

where w represents contact width between shaft and bearing along the axial direction.

In practical engineering applications, wear depth can describe wear characteristics more conveniently than wear volume. Therefore, dividing equation (25) by the actual contact area A_a, we can get the following [5, 24]:

$$\frac{h}{s} = k\frac{p}{H} = k_d p, \tag{29}$$

where k_d is the linear wear coefficient, $k_d = k/H$, h is the wear depth, and p is the contact stress.

Equation (25) is the most commonly used expression of Archard's model. However, the wear procedure is generally regarded as a dynamic process. Therefore, contact point of pair continuously changes during motion of mechanism,

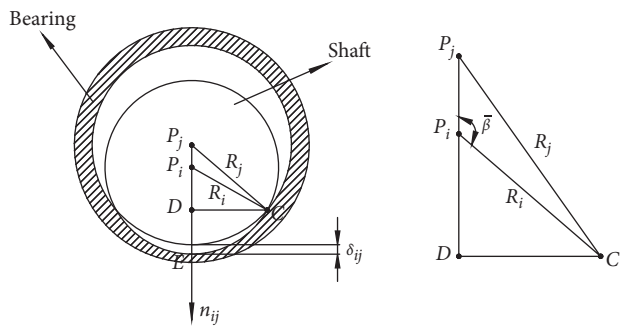

Figure 3: Contact form and geometric relationship of revolute joint considering clearance.

and frequent contact areas usually occur in some special contact locations, which result in irregular contact wear rather than uniform wear of elements in clearance joints. In addition, the sliding distance of contact collision points of contact elements of clearance joint changes with the dynamic contact force. Therefore, the dynamic wear characteristics of the multibody system with clearances are generally studied in differential form [5, 19, 24]:

$$dh = k_d p\, ds. \tag{30}$$

Equation (30) is updated via a temporal discretization of relative motion of contact components, and the wear depth of m cycles can be written as follows [18, 22, 25]:

$$h_m = h_{m-1} + \Delta h_m, \tag{31}$$

where h_{m-1} represents the wear depth at the previous cycle and Δh_m represents the wear depth at the mth cycle.

4.2. Surface Reconstruction after Wear for Revolute Clearance Joint. Based upon thought of the finite element method, the geometric surface of shaft and bearing are discretized. In every integral time step, the contact condition between shaft and bearing is judged. When shaft contacts with bearing, the location (discrete region) where the shaft contacts with bearing is stored and wear depth at this location is also calculated. Finally, the amount of wear depth accumulated on a discrete region is the sum of all partial wear depths at each integral time step of this discrete region. By this method, new geometry of the joint surface caused by wear can be calculated.

Therefore, the total amount of the wear depth could be written as follows [18, 23]:

$$h = \sum h_n, \tag{32}$$

where n represents the code name of discrete region in which the joint surface is divided and h_n is the wear depth at the nth discrete region.

It is assumed that the surface material of the shaft and bearing is same and wear depth in shaft is equal to wear depth in bearing. Wear depth values of shaft and wearing are both set as half of the total wear depth. Based upon revolute pair geometric properties, new journal and bearing radius at each discrete region after wear can be given by the following equation [20, 23]:

$$\begin{cases} R_i^* = R_i - \dfrac{h}{2}, \\ R_j^* = R_j + \dfrac{h}{2}. \end{cases} \tag{33}$$

4.3. Dynamic Analysis and Wear Analysis Integration. The main calculation processes for the mechanics system containing revolute pair wear include dynamics research and wear analysis. In order to forecast the effect of wear at revolute pair on dynamic characteristics, it is important to integrate the wear model with the dynamic model considering clearance and analyzing the effect of wear on dynamic responses.

It is noteworthy that the clearance value is no longer a constant after wear, and it depends on the radius of the new bearing and shaft at this contact region. The clearance in this contact region after wear could be expressed as

$$c^*(n) = R_i^*(n) - R_j^*(n). \tag{34}$$

Once clearance value at this contact region is obtained, penetration depth of this region could be obtained by using equation (3). In addition, the contact force model could be updated with new sizes of the radius of bearing and shaft; that is, the stiffness coefficient defined in equation (8) can be updated according to new radius of bearings and shafts. The stiffness coefficient after wear could be expressed as follows:

$$K^*(n) = \frac{4}{3\pi\left(\sigma_i + \sigma_j\right)} \left(\frac{R_i^*(n) R_j^*(n)}{R_i^*(n) + R_j^*(n)} \right)^{1/2}. \tag{35}$$

The dynamic and wear integration frame is shown in Figure 4.

5. Dynamic Response Analysis of 2-DOF Nine-Bar Mechanism with Revolute Clearances

When the number of cycles for the mechanism is small, wear depth and clearance value change little. If the surface of the shaft and bearing is reconstructed after each contact, the calculation cost will be greatly increased and the efficiency will be very low. Therefore, assumptions are set as follows:

(1) It is assumed that the surface of the shaft and bearing does not change with time in a certain operating periods. Supposing that the mechanism runs every 100 cycles, wear is calculated once and surface of shaft and bearing is reconstructed once. Because the wear amount produced in 100 cycles is too little, the surface reconstruction is not clear, and if mechanism runs two million cycles, it will waste a lot of time, so the 100 cycles are magnified 20,000 times to approximate the mechanism running 2 million cycles in this paper.

(2) It is assumed that shaft and bearing surfaces are divided into 1000 discrete regions.

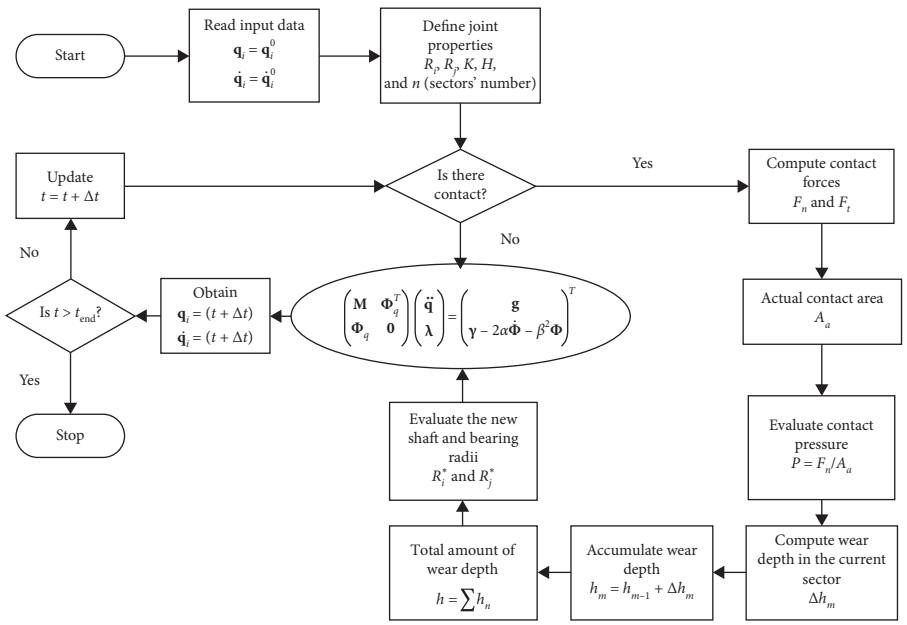

Figure 4: The dynamic and wear integration frame.

Table 1: Dimensions and mass properties.

Component	Crank 1	Rod 2	Rod 3	Crank 4	Rod 5	Rod 6	Triangular panel 7			Rod 8	Slider 9
Length (mm)	L_1 45	L_2 326	L_3 497	L_4 95	L_5 430	L_6 230	L_{71} 45	L_{72} 326	L_{73} 497	L_8 95	—
	L_{s1} 23	L_{s2} 163	L_{s3} 249	L_{s4} 48	—	L_{s6} 115		L_{s7} 147		L_{s8} 168	
Mass (g)	148	805	603	265	—	581		4334		827	801
Moment of inertia (10^{-3}kg·m^2)	0.2382	8.001	13.37	1.210	—	12.12		3.802		8.663	—

Table 2: Clearance joints' parameters.

Designed parameter	Parameter values
Bearing radius R_1 (mm)	15
Restitution coefficient c_e	0.9
Elastic moduli E_i and E_j (GPa)	200
Poisson's ratios v_i and v_j	0.3
Baumgarte stabilization coefficient α	5
Baumgarte stabilization coefficient β	5
Bristle stiffness σ_0 (N/m)	100,000
Microscopic damping coefficient σ_1 (Ns/m)	400
Viscous friction coefficient σ_2	0
Stribeck velocity v_s	1% of maximum v_t
Gradient of friction decay γ	2
Linear wear coefficient	8×10^{-14} Pa^{-1}
Integral step (s)	0.0001
Relative tolerance	0.000001

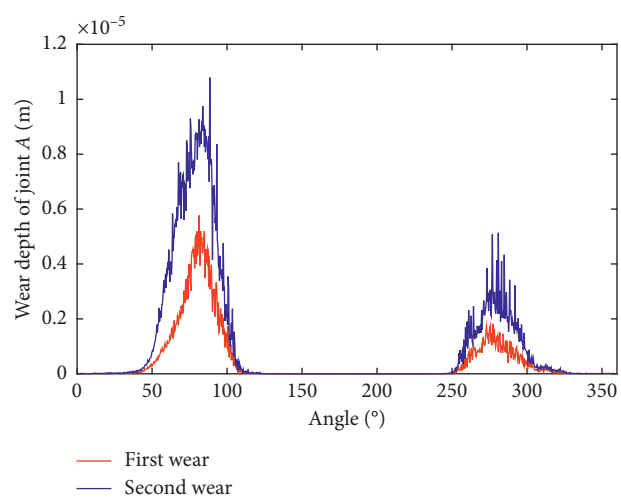

Figure 5: Wear depth of joint A.

(3) It is assumed that the surface material of shaft and bearing is the same, and the wear depth in shaft is equal to wear depth in bearing, which is half of the total wear depth.

Based upon above, the wear phenomenon of revolute clearance joints of 2-DOF nine-bar mechanism is studied and the surface of shaft and bearing after wear is also reconstructed. The dynamic responses of 2-DOF nine-bar mechanism considering constant and nonregular revolute clearances caused by wear are also both researched. Influences of different initial constant clearance values and

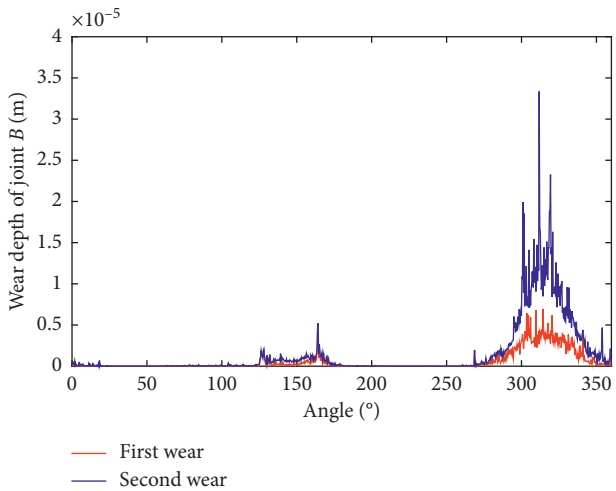

Figure 6: Wear depth of joint B.

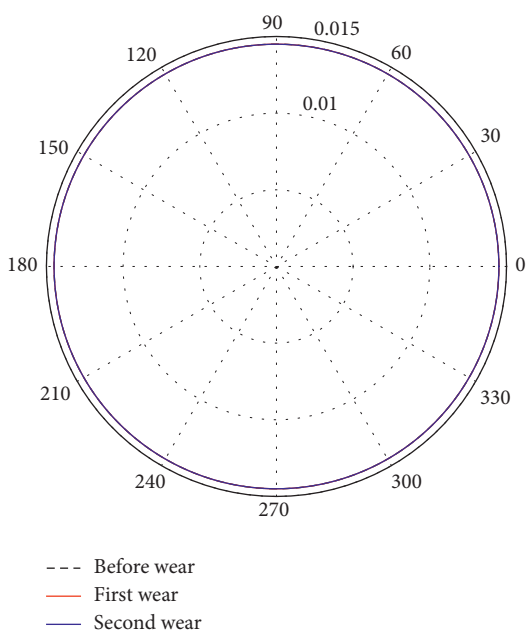

Figure 7: Shaft surface of joint A.

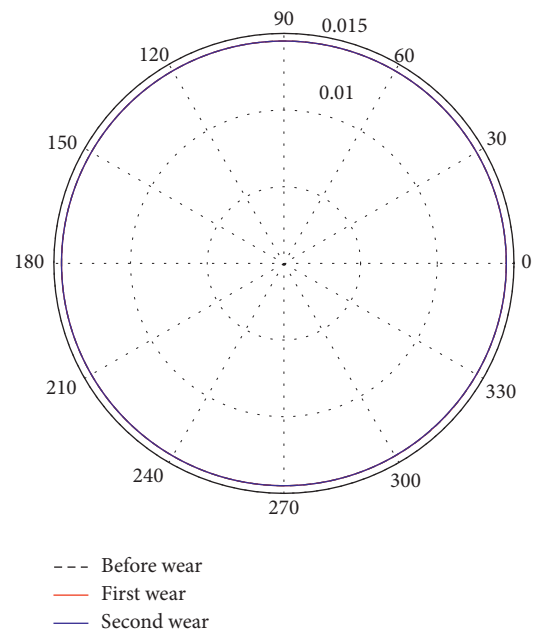

Figure 8: Shaft surface of joint B.

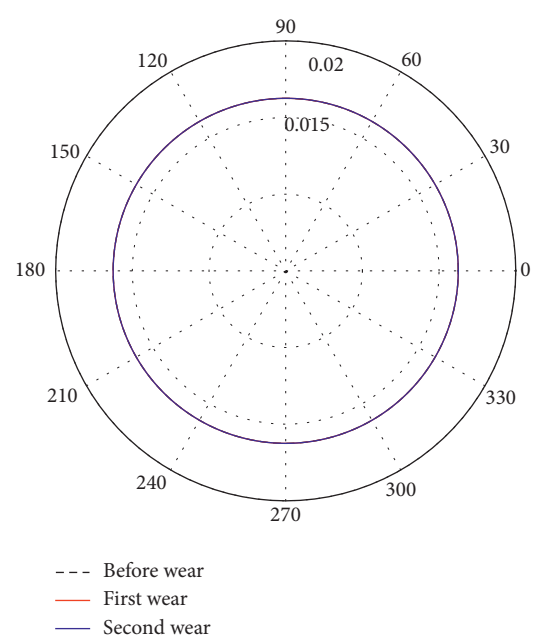

Figure 9: Bearing surface of joint A.

different driving speeds on wear are also researched. Ode15s function in MATLAB is used to solve the dynamic equation.

5.1. System Parameters. The system parameters are illustrated in Tables 1 and 2.

5.2. Wear Prediction and Dynamic Analysis. It is assumed that speeds of crank 1 and crank 4 are, respectively, -2π (rad/s) and 2π (rad/s). And the constant clearance size before wear of two revolute clearance joints are both set as 0.5 mm.

5.2.1. Wear Prediction. Wear depth at joint A and joint B is displayed in Figures 5 and 6. The reconstructed surface of shaft A, shaft B, bearing A, and bearing B after wear is shown in Figures7–10, respectively. Local enlarged drawing of the reconstructed surface of shaft A, shaft B, bearing A, and bearing B is shown in Figures 11–14, respectively.

After the first wear cycle of the mechanism, according to the wear depth of the first wear cycle, the process of reconstructing the surface of the shaft and bearing for the first time is called the first wear. After the second wear cycle of the mechanism, the wear depth corresponding to the second wear cycle is generated. On the surface of the shaft and bearing formed after the first wear, the process of

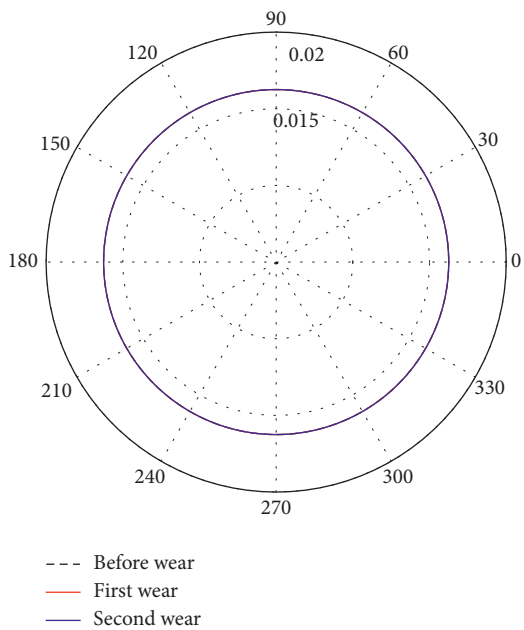

Figure 10: Bearing surface of joint B.

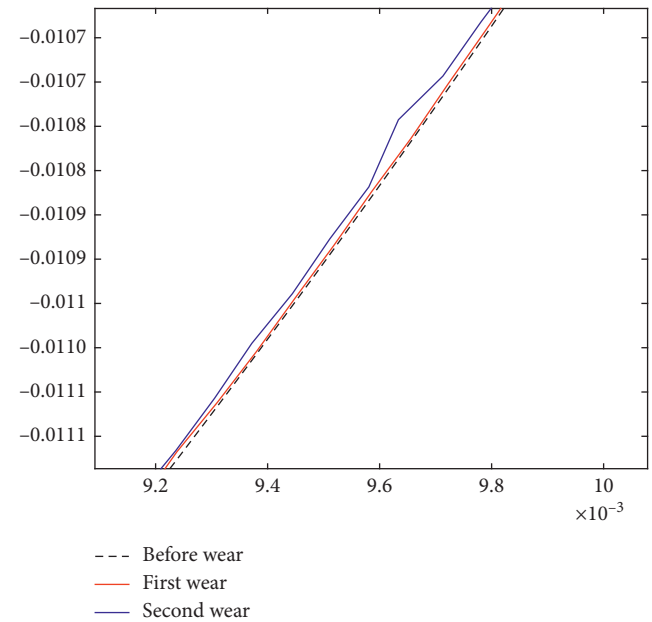

Figure 12: Local enlarged drawing of the shaft surface of joint B.

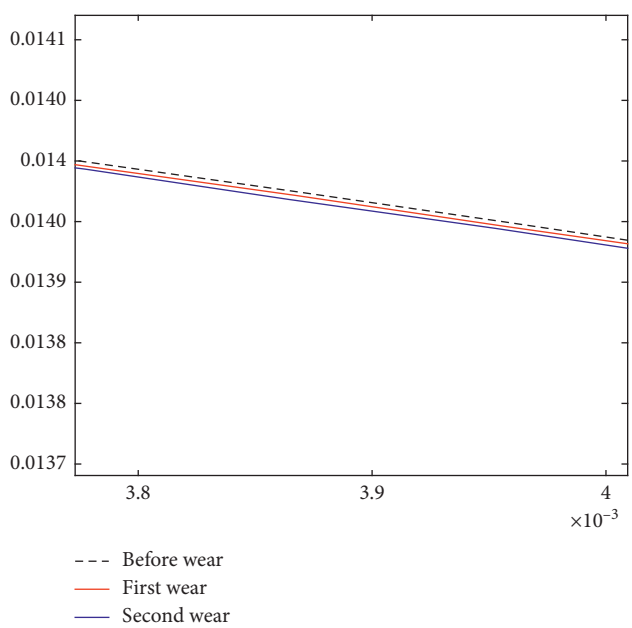

Figure 11: Local enlarged drawing of the shaft surface of joint A.

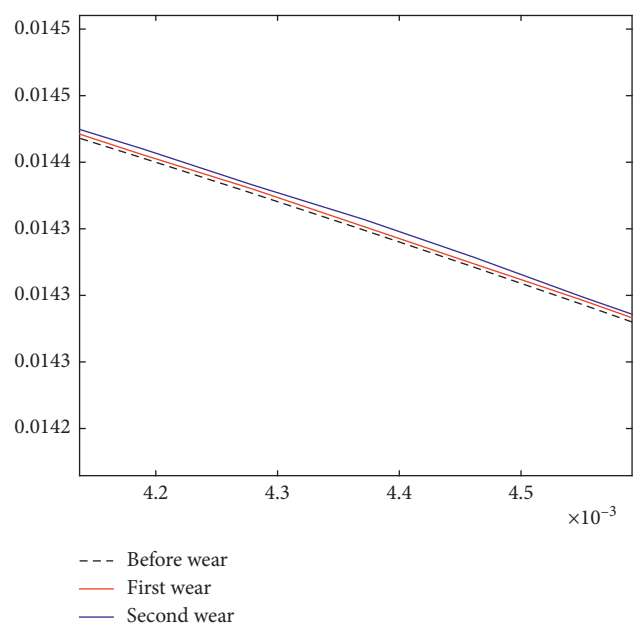

Figure 13: Local enlarged drawing of the bearing surface of joint A.

reconstructing the surface of the shaft and bearing for the second time is called the second wear.

From Figures 5 and 6, it can be seen that the wear depth of the second wear is obviously higher than that of the first wear, wear depth at revolute joint B is greater than that of revolute joint A, the wear is more serious, and the wear range is more widely.

The wear depths of first wear and second wear at revolute joint A are 5.768×10^{-6} m and 1.079×10^{-5} m, respectively. The wear depths of first wear and second wear at revolute joint B are 6.965×10^{-6} m and 3.336×10^{-5}m, respectively. As can be seen from Figure 5, the wear area of joint A is mainly in [32°, 120°] and [246°, 328°]. As shown in Figure 7, the wear area of joint B is mainly focused on [0°, 20°], [123°, 180°], and [260°, 360°]. This is mainly due to frequent contact between shaft and bearing in these regions. From Figures 7–14, the wear is not obvious on the surface of bearings and shafts due to the wear depths of two revolute clearances are too small. It can be seen from the local enlargement diagram that the surface damage of shaft and bearing after the second wear is more serious than that of the first wear.

5.2.2. Influence of Clearance Wear on Dynamic Responses. The dynamics analyses of 2-DOF nine-bar mechanism with constant revolute clearance values and nonregular revolute

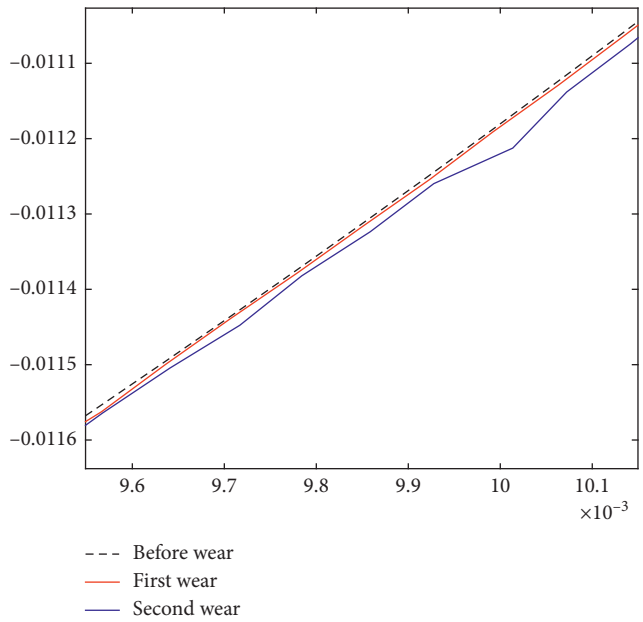

Figure 14: Local enlarged drawing of the bearing surface of joint B.

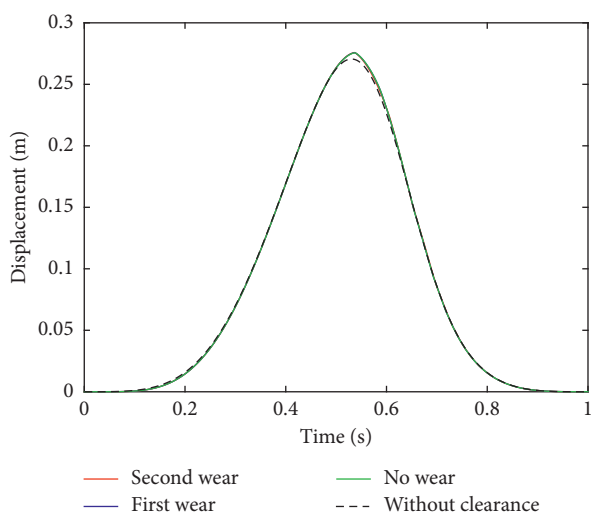

Figure 15: Slider's displacement.

clearance values caused by wear (including first wear and second wear) are developed. The motion characteristics of the end slider are shown in Figures 15–20, including the slider's displacement, slider's displacement error, slider's velocity, slider's velocity error, slider's acceleration, and slider's acceleration error. Input torques of cranks, contact forces at revolute clearance joints, and shaft trajectories of revolute clearance pairs are illustrated in Figures 21–26.

According to Figures 15 and 16, influence of the revolute clearances on displacement of the slider is very small, which is in good agreement with the displacement curve under mechanism without clearances. As can be seen from Figures 17 and 18, clearance joints have influence on the speed of slider. Compared with the case without clearance, obvious vibration can be seen in Figure 17. It can be concluded from

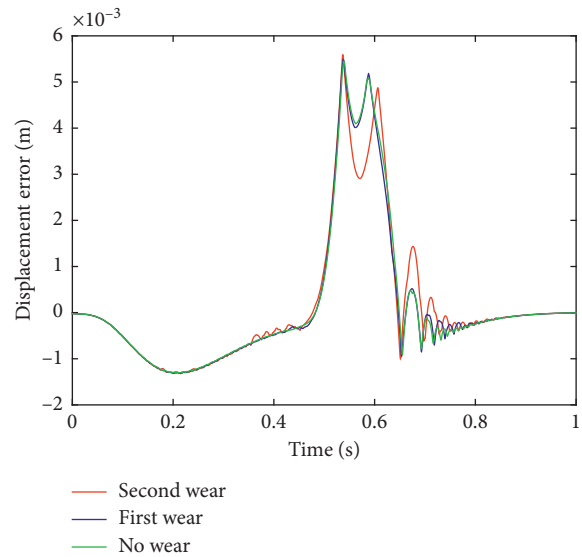

Figure 16: Slider's displacement error.

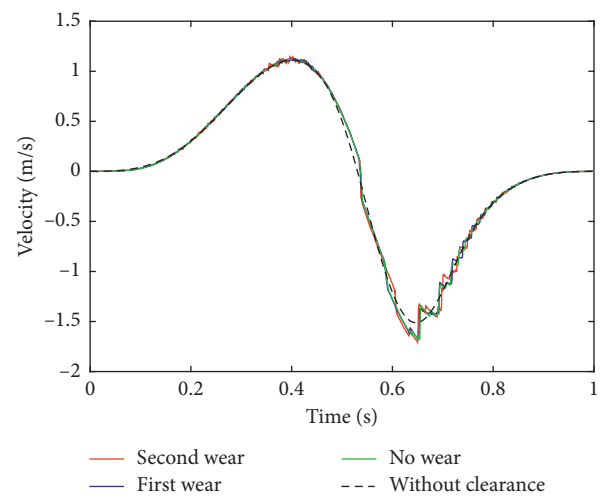

Figure 17: Slider's velocity.

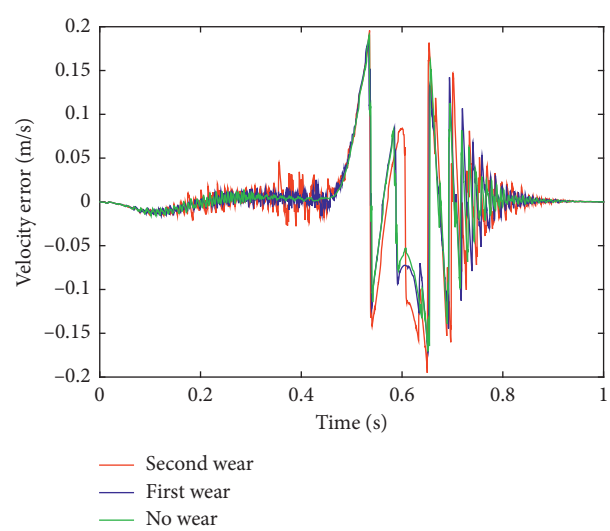

Figure 18: Slider's velocity error.

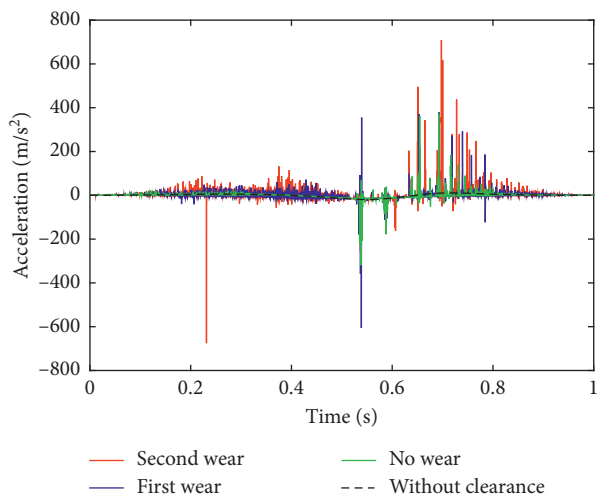

Figure 19: Slider's acceleration.

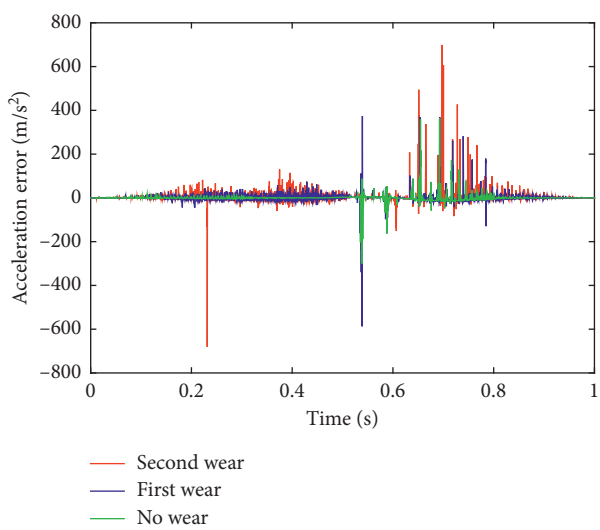

Figure 20: Slider's acceleration error.

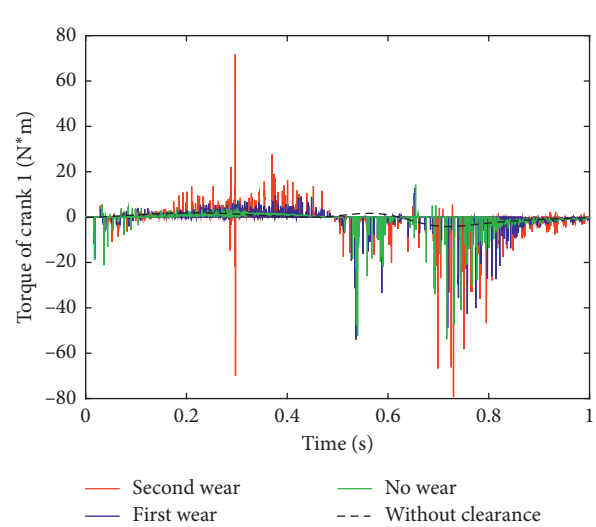

Figure 21: Input torque of crank 1.

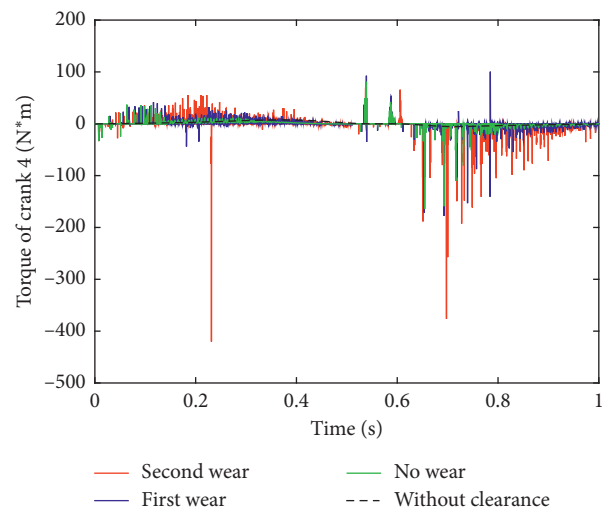

Figure 22: Input torque of crank 4.

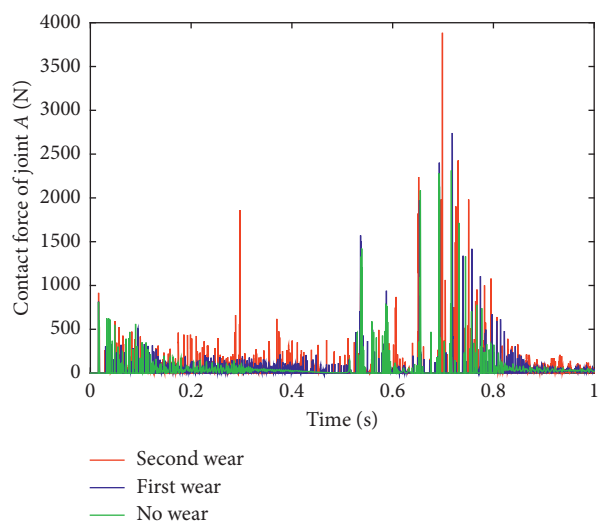

Figure 23: Contact force of joint A.

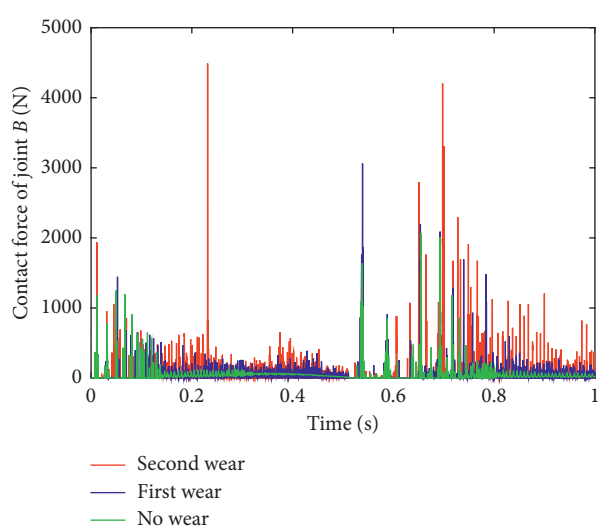

Figure 24: Contact force of joint B.

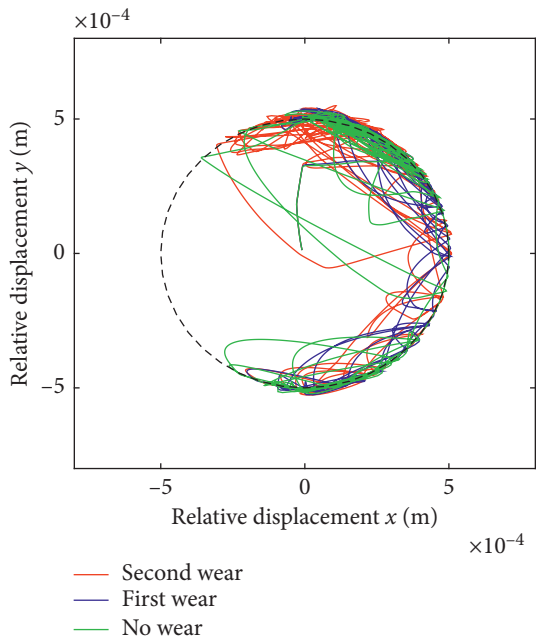

Figure 25: Shaft trajectory of joint A.

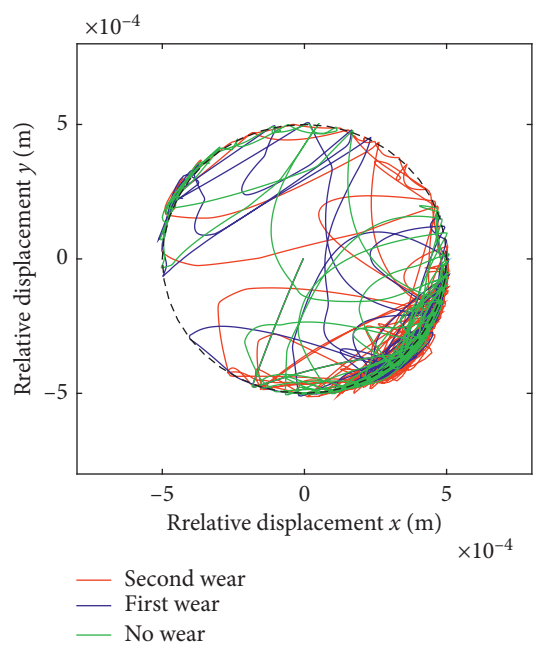

Figure 26: Shaft trajectory of joint B.

the velocity error diagram (Figure 18) that the vibration frequency of velocity increases with the increase of wear times. However, from Figures 19–24, the revolute clearances have a great influence on slider's acceleration, contact forces, and input torques, which produce huge peak value and violent vibration, mainly due to impact between shaft and bearing at clearance pairs.

It can be seen from the figure that the peak values of dynamic responses and vibration after wear increased and intensified compared with those without wear. Moreover, dynamic responses of second wear are more obvious than that of first wear. The peak value of acceleration of slider, contact force of joint A, contact force of joint B, input torque of crank 1, and input torque of crank 4 of no wear are 372.4 m/s^2, 2072 N, 2314 N, −52.33 N ∗ m, and −164.3 N ∗ m. The peak value of acceleration of slider, contact force of joint A, contact force of joint B, input torque of crank 1, and input torque of crank 4 of first wear are −606.1 m/s^2, 2741 N, 3062 N, −53.38 N ∗ m, and −177.5 N ∗ m. The peak value of acceleration of slider, contact force of joint A, contact force of joint B,

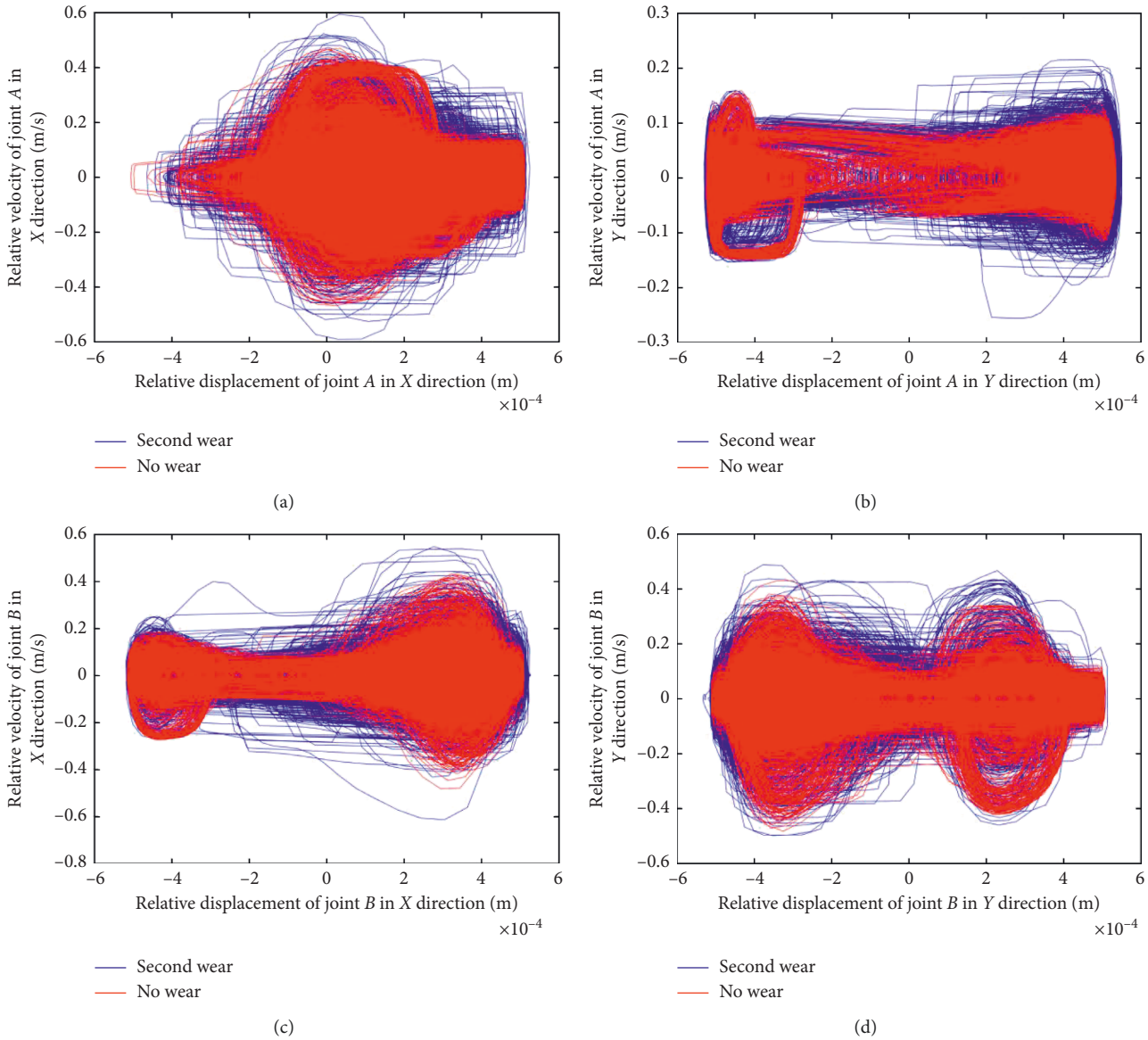

Figure 27: Phase diagram of (a) joint A in the X direction, (b) joint A in the Y direction, (c) joint B in the X direction, and (d) joint B in the Y direction.

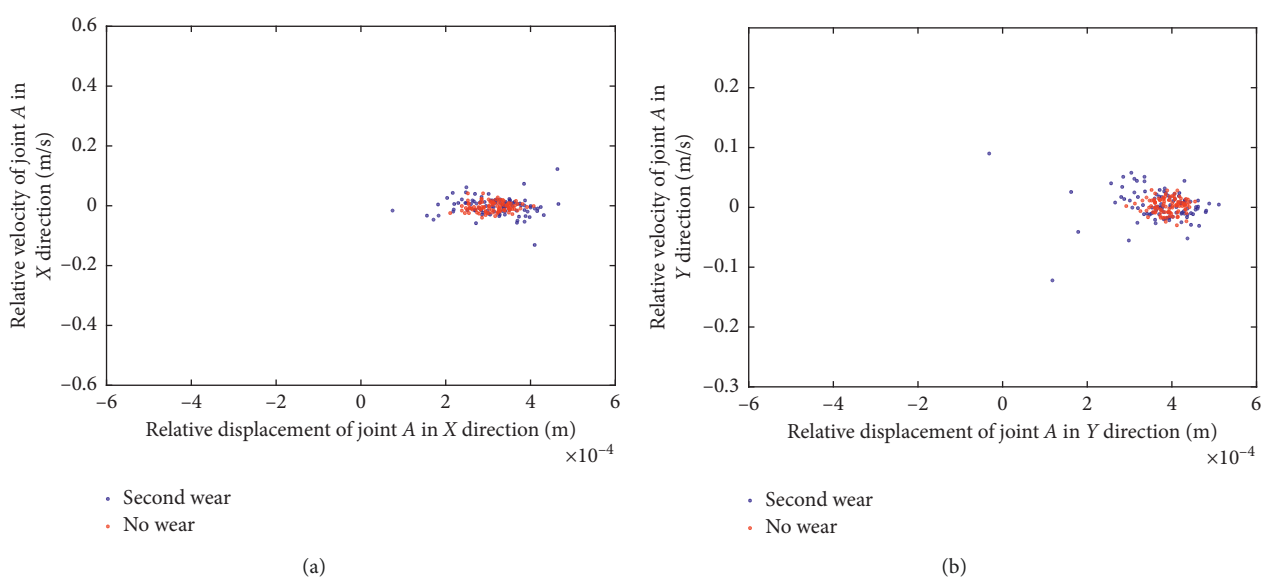

Figure 28: Continued.

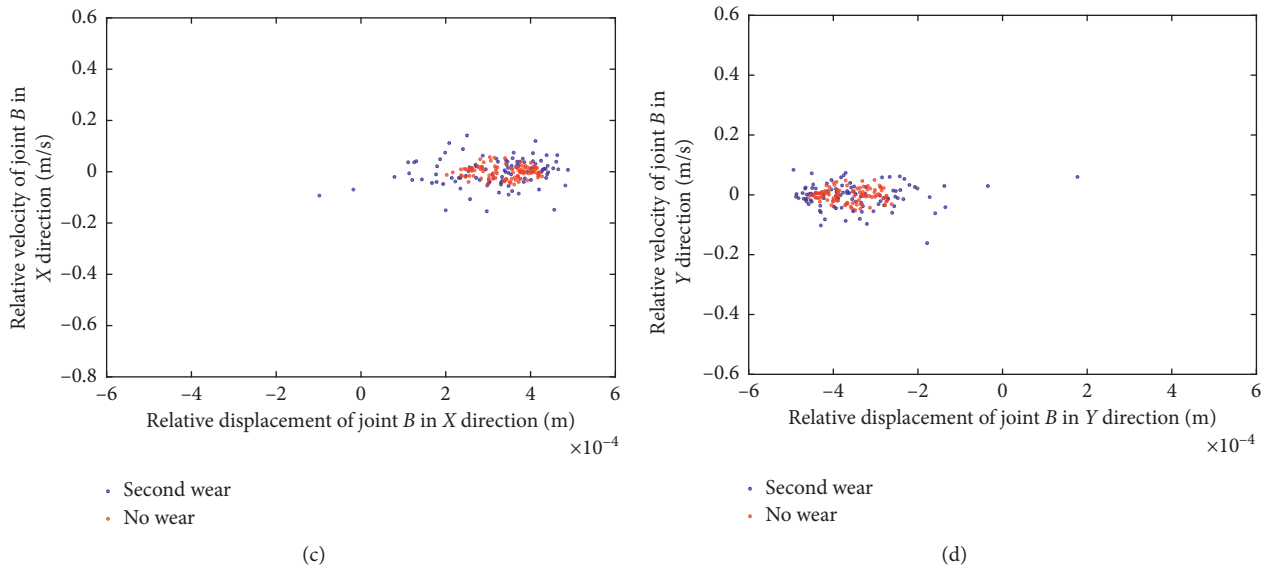

Figure 28: Poincaré map of (a) joint A in the X direction, (b) joint A in the Y direction, (c) joint B in the X direction, and (d) joint B in the Y direction.

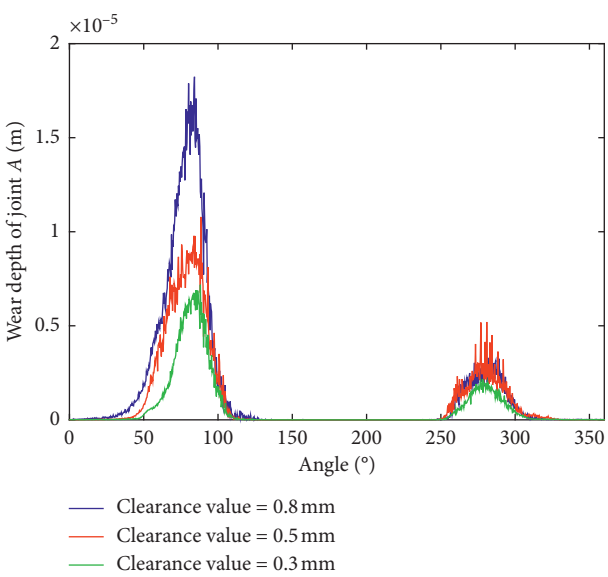

Figure 29: Wear depth at joint A.

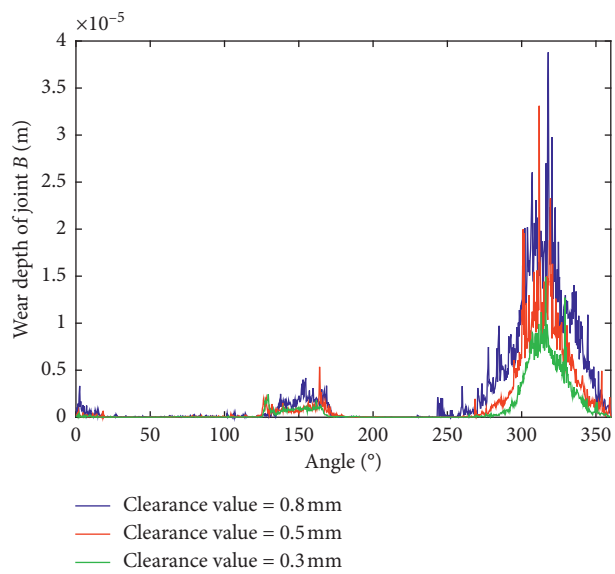

Figure 30: Wear depth at joint B.

input torque of crank 1, and input torque of crank 4 of second wear are 708.7 m/s^2, 3885 N, 4489 N, −79.34 N ∗ m, and −420.2 N ∗ m. As displayed in Figures 25 and 26, with the increase of wear times, shaft trajectories of clearance joints become more and more chaotic. It is shown that wear has a greater impact on dynamic response, which will accelerate damage and failure for mechanism. Reasons are that clearance pair wear is nonuniform, and the clearance value is changed larger and nonregularly after clearance joint wear.

5.2.3. Influence of Clearance Wear on Nonlinear Dynamic Characteristics. Clearance wear will destroy the revolute joint with clearance, so it has great influence on the nonlinear dynamics of the mechanism. The nonlinear characteristics of the mechanism before wear and after second wear are both studied by using the phase diagram and Poincaré map. The phase diagram and Poincaré map are shown in Figures 27 and 28.

It can be seen from the phase diagram and Poincaré map that wear enlarges the area of the phase diagram and makes the range of Poincaré map point diffuse. Moreover, the distribution of mapping points after wear is more confused. The chaotic phenomena at the clearance joint are enhanced by the wear. The reason is that wear makes the surface of shaft and bearing not smooth and increases the impact and vibration between elements of clearance pair.

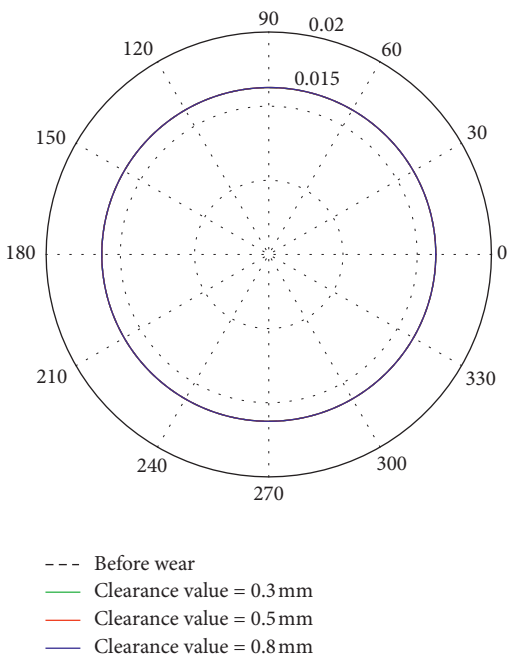

Figure 31: Bearing surface of joint A.

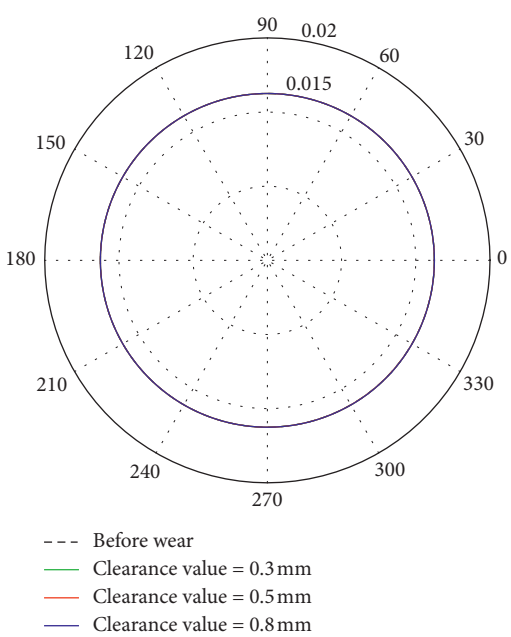

Figure 32: Local enlarged drawing of bearing surface of joint A.

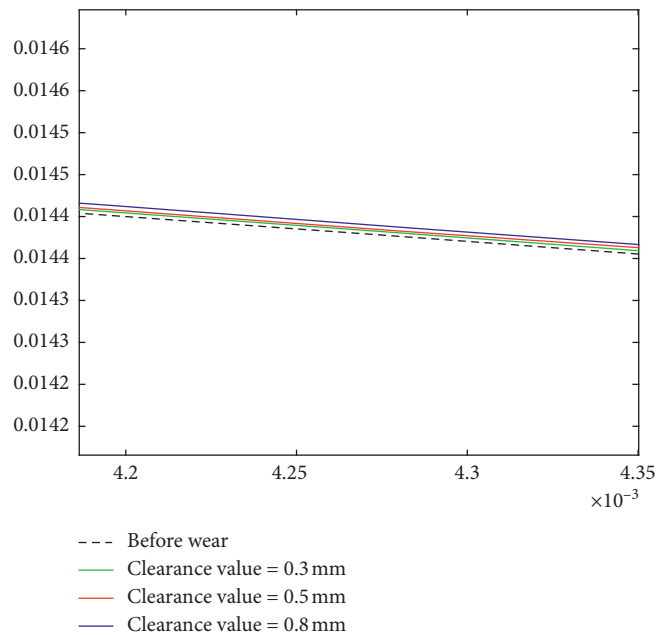

Figure 33: Bearing surface of joint B.

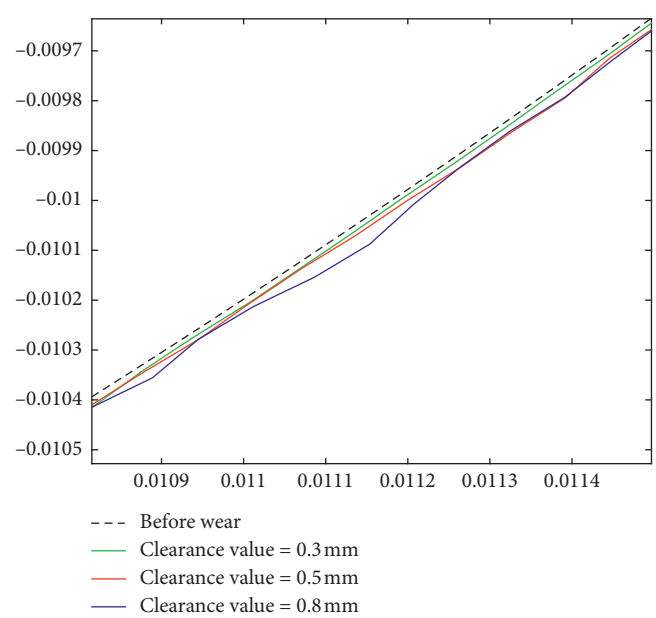

Figure 34: Local enlarged drawing of bearing surface of joint B.

5.3. The Influence of Different Factors on Wear

5.3.1. The Effect of Different Initial Constant Clearance Sizes on Wear. The effect of three different initial constant clearance values on wear analysis is investigated in this section. It is assumed that revolute pair A and revolute pair B have the same clearance value. It is supposed that driving speeds of crank 1 $\omega_1 = -2\pi\,(\text{rad/s})$ and crank 4 $\omega_4 = 2\pi\,(\text{rad/s})$. Initial constant clearance values 0.3 mm, 0.5 mm, and 0.8 mm are all selected to study the wear analysis. Wear depths at joint A and joint B are displayed in Figures 29 and 30. The reconstructed surface of bearing A and bearing B after wear is shown in Figures 31 and 32. Local enlarged drawing of the reconstructed surface of bearing A and bearing B is shown in Figures 33 and 34. The figures are drawn on the basis of the data after the second wear in this section.

From Figures 29–34, it can be seen that, because of frequent collisions in some areas, wear phenomenon on bearing surface is not uniformly distributed. And the wear of revolute joint B is more serious than revolute joint A. As shown in Figures 29 and 30, the greater the constant clearance before wear is, the greater the wear depth is, the enlarger the wear area

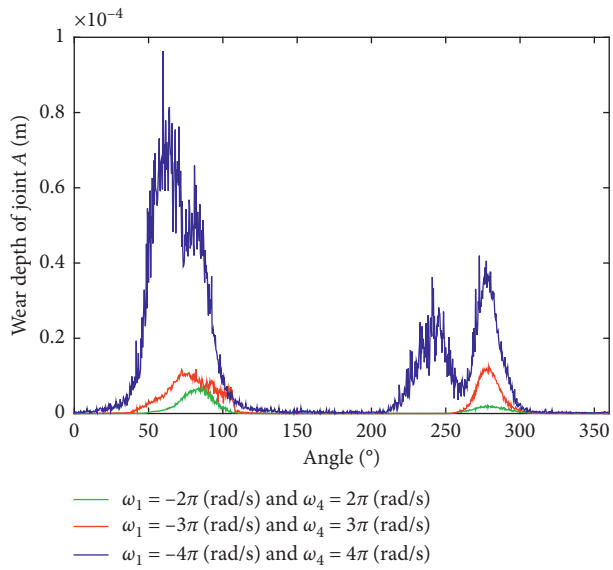

Figure 35: Wear depth at joint A.

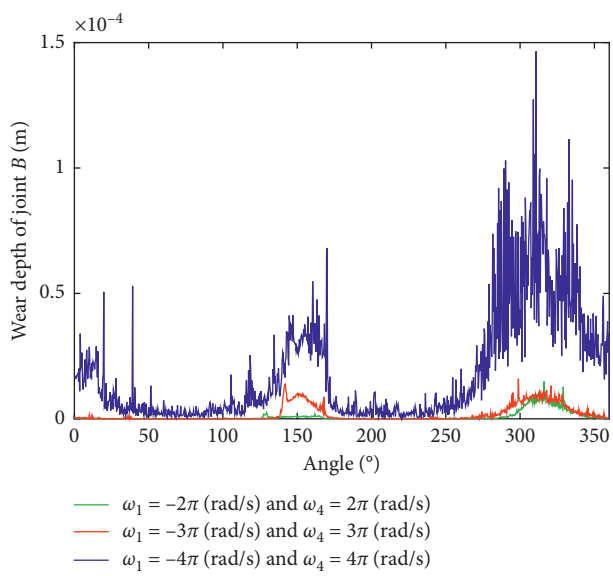

Figure 36: Wear depth at joint B.

is, and the worse the wear of shaft and bearing are. When the initial constant clearance values are 0.3 mm, 0.5 mm, and 0.8 mm, the corresponding wear depths of revolute A are 1.824×10^{-5} m, 1.079×10^{-5} m, and 7.182×10^{-6}m, and the corresponding wear depths of revolute B are 3.881×10^{-5} m, 3.336×10^{-5} m, and 1.492×10^{-5} m, respectively. It can be guessed that proper reduction of the clearance value at the rotating pair is beneficial to the reduction of wear phenomenon. The wear at revolute clearance joints seriously degenerate precision and reliability of the multibody mechanism system.

5.3.2. The Effect of Different Driving Speeds on Wear. Influences of three different driving speeds on wear analyses are researched in this section. It is supposed that constant clearance values at two revolute clearance joints before wear are both set as

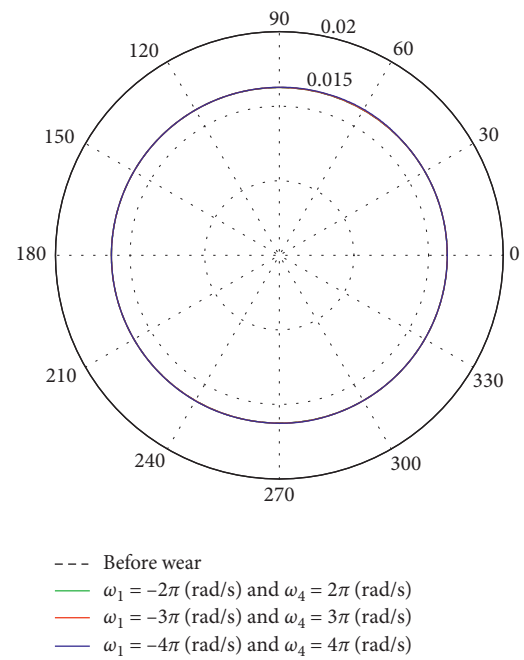

Figure 37: Bearing surface of joint A.

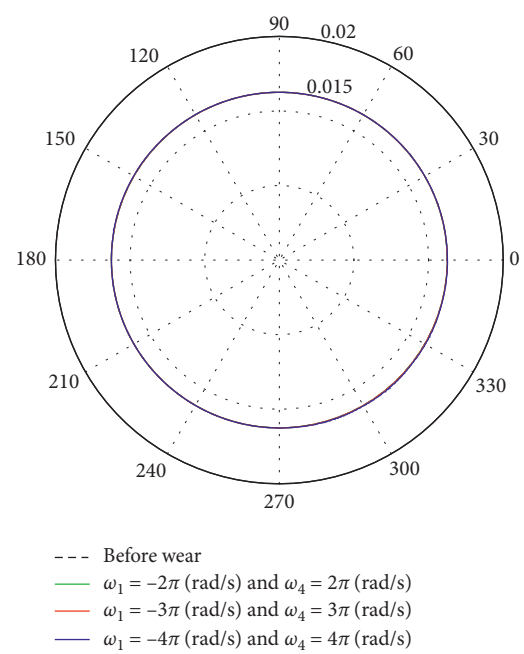

Figure 38: Bearing surface of joint B.

0.3 mm. Driving speed of crank 1 and crank 4 is chosen as $\omega_1 = -2\pi\,(\mathrm{rad/s})$ and $\omega_4 = 2\pi\,(\mathrm{rad/s})$, $\omega_1 = -3\pi\,(\mathrm{rad/s})$ and $\omega_4 = 3\pi\,(\mathrm{rad/s})$, and $\omega_1 = -4\pi\,(\mathrm{rad/s})$ and $\omega_4 = 4\pi\,(\mathrm{rad/s})$. Wear depth at joints A and B is displayed in Figures 35 and 36. The reconstructed surface of bearing A and bearing B after wear is shown in Figures 37 and 38. Local enlarged drawing of the reconstructed surface of bearing A and bearing B is shown in Figures 38 and 39. The figures are also drawn on the basis of the data after the second wear in this section.

With the increase of driving speed, the clearances at the revolute joints will make the collision of the

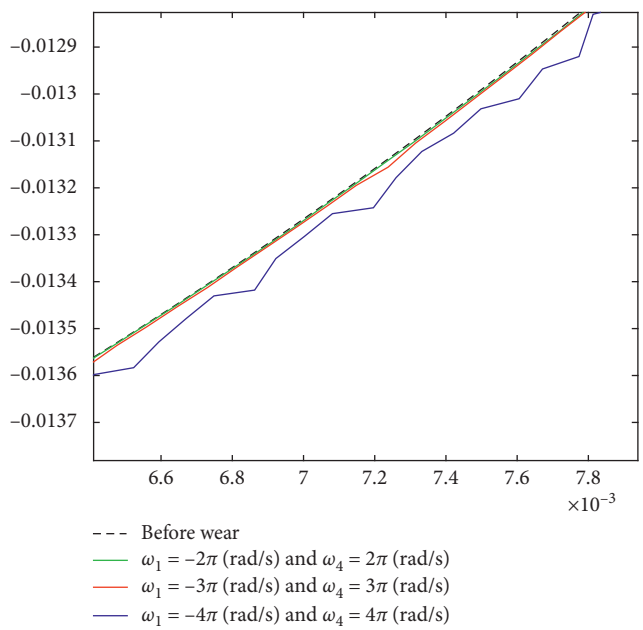

Figure 39: Local enlarged drawing of bearing surface of joint B.

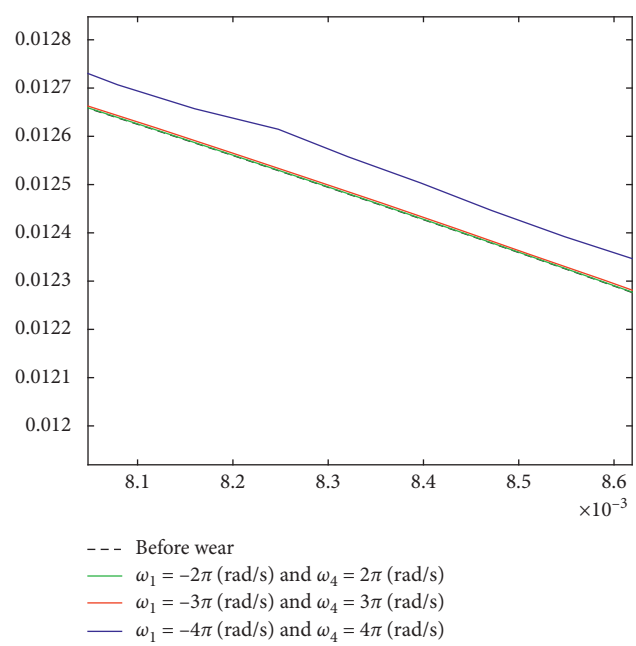

Figure 40: Local enlarged drawing of bearing surface of joint A.

mechanism more intense, accelerate the damage of mechanism, and reduce life of the mechanism. According to Figures 35–40, the wear of revolute joint B is more severe than that of revolute joint A, the greater the driving speed is, the greater the wear depth is, the worse wear on the bearing surface is, and the faster failure of the mechanism is. When the driving speeds are $\omega_1 = -2\pi\,(\mathrm{rad}/s)$ and $\omega_4 = 2\pi\,(\mathrm{rad}/s)$, $\omega_1 = -3\pi\,(\mathrm{rad}/s)$ and $\omega_4 = 3\pi\,(\mathrm{rad}/s)$, and $\omega_1 = -4\pi\,(\mathrm{rad}/s)$ and $\omega_4 = 4\pi\,(\mathrm{rad}/s)$, the corresponding wear depths of revolute A are 9.673×10^{-5} m, 1.237×10^{-5}m, and 7.182×10^{-6} m, respectively. When the clearance values are $\omega_1 = -2\pi\,(\mathrm{rad}/s)$ and $\omega_4 = 2\pi\,(\mathrm{rad}/s)$, $\omega_1 = -3\pi\,(\mathrm{rad}/s)$ and $\omega_4 = 3\pi\,(\mathrm{rad}/s)$, and $\omega_1 = -4\pi\,(\mathrm{rad}/s)$ and $\omega_4 = 4\pi\,(\mathrm{rad}/s)$, the corresponding wear depths of revolute B are 1.465×10^{-4} m, 1.599×10^{-5} m, and 1.492×10^{-5} m, respectively. After the clearance wear, clearance values of revolute joints are increased and not a constant value, which will cause the high-frequency vibration of dynamic responses. The driving speed will directly affect the relative motion state between elements of clearance pair, and it has impact on the wear of clearance pair.

6. Conclusions

The planar 2-DOF nine-bar mechanism is utilized as an example to investigate dynamic responses of the mechanical system considering two revolute clearance joints after twice wear. Main contents are as follows:

(1) Dynamic equation of 2-DOF nine bar mechanism considering two revolute clearance joints by combining the L-N model and LuGre model is established.

(2) Based upon Archard's model, wear depths of two revolute clearance joints are predicted, and the surface of shaft and bearing is reconstructed twice.

(3) By integrating the wear model with the dynamic model, the dynamic responses of 2-DOF nine-bar mechanism considering two revolute clearances wear are both discussed. The nonlinear characteristics of the mechanism after wear are studied by the phase diagram and Poincaré map.

(4) The influences of different initial constant clearance values and driving speed of cranks on wear of two revolute clearance joints are also investigated.

Data Availability

The data used to support the findings of this study are included within the article.

Conflicts of Interest

The authors declare that they have no conflicts of interest.

Acknowledgments

This paper was supported by the Shandong Key Research and Development Public Welfare Program (2019GGX104011), Natural Science Foundation of Shandong Province (Grant no. ZR2017MEE066), the Open Project of Heavy-Duty Intelligent Manufacturing Equipment Innovation Center of Hebei Province (201904), and the Graduate Innovation Project of Shandong University of Science and Technology (no. SDKDYC190221).

References

[1] P. Flores, "A parametric study on the dynamic response of planar multibody systems with multiple clearance joints," *Nonlinear Dynamics*, vol. 61, no. 4, pp. 633–653, 2010.

[2] L. Tang and J. Liu, "Modeling and analysis of sliding joints with clearances in flexible multibody systems," *Nonlinear Dynamics*, vol. 94, no. 4, pp. 2423–2440, 2018.

[3] Q. Liu, S.-N. Lu, and X.-L. Ding, "An error equivalent model of revolute joints with clearances for antenna pointing mechanisms," *Chinese Journal of Mechanical Engineering*, vol. 31, no. 1, pp. 31–39, 2018.

[4] N. Akhadkar, V. Acary, and B. Brogliato, "Multibody systems with 3D revolute joints with clearances: an industrial case study with an experimental validation," *Multibody System Dynamics*, vol. 42, no. 3, pp. 249–282, 2018.

[5] P. Li, W. Chen, and A. Zhu, "An improved practical model for wear prediction of revolute clearance joints in crank slider mechanisms," *Science China Technological Sciences*, vol. 56, no. 12, pp. 2953–2963, 2013.

[6] A. Zhu, S. He, J. Zhao, and W. Luo, "A nonlinear contact pressure distribution model for wear calculation of planar revolute joint with clearance," *Nonlinear Dynamics*, vol. 88, no. 1, pp. 315–328, 2017.

[7] X. Lai, H. He, Q. Lai et al., "Computational prediction and experimental validation of revolute joint clearance wear in the low-velocity planar mechanism," *Mechanical Systems and Signal Processing*, vol. 85, pp. 963–976, 2017.

[8] H. Tan, Y. Hu, and L. Li, "A continuous analysis method of planar rigid-body mechanical systems with two revolute clearance joints," *Multibody System Dynamics*, vol. 40, no. 4, pp. 347–373, 2017.

[9] G. Wang, Z. Qi, and J. Wang, "A differential approach for modeling revolute clearance joints in planar rigid multibody systems," *Multibody System Dynamics*, vol. 39, no. 4, pp. 311–335, 2017.

[10] Y. Chen, Y. Sun, and C. Chen, "Dynamic analysis of a planar slider-crank mechanism with clearance for a high speed and heavy load press system," *Mechanism and Machine Theory*, vol. 98, pp. 81–100, 2016.

[11] Z. Wang, Q. Tian, H. Hu, and P. Flores, "Nonlinear dynamics and chaotic control of a flexible multibody system with uncertain joint clearance," *Nonlinear Dynamics*, vol. 86, no. 3, pp. 1571–1597, 2016.

[12] E. Zheng, R. Zhu, S. Zhu, and X. Lu, "A study on dynamics of flexible multi-link mechanism including joints with clearance and lubrication for ultra-precision presses," *Nonlinear Dynamics*, vol. 83, no. 1-2, pp. 137–159, 2016.

[13] O. Muvengei, J. Kihiu, and B. Ikua, "Dynamic analysis of planar rigid-body mechanical systems with two-clearance revolute joints," *Nonlinear Dynamics*, vol. 73, no. 1-2, pp. 259–273, 2013.

[14] P. Flores, J. Ambrósio, J. C. P. Claro, and H. M. Lankarani, "Dynamic behaviour of planar rigid multi-body systems including revolute joints with clearance," *Proceedings of the Institution of Mechanical Engineers, Part K: Journal of Multi-Body Dynamics*, vol. 221, no. 2, pp. 161–174, 2007.

[15] X. Chen, S. Jiang, Y. Deng, and Q. Wang, "Dynamics analysis of 2-DOF complex planar mechanical system with joint clearance and flexible links," *Nonlinear Dynamics*, vol. 93, no. 3, pp. 1009–1034, 2018.

[16] S. Yaqubi, M. Dardel, H. M. Daniali, and M. H. Ghasemi, "Modeling and control of crank-slider mechanism with multiple clearance joints," *Multibody System Dynamics*, vol. 36, no. 2, pp. 143–167, 2016.

[17] O. Muvengei, J. Kihiu, and B. Ikua, "Dynamic analysis of planar multi-body systems with LuGre friction at differently located revolute clearance joints," *Multibody System Dynamics*, vol. 28, no. 4, pp. 369–393, 2012.

[18] P. Flores, "Modeling and simulation of wear in revolute clearance joints in multibody systems," *Mechanism and Machine Theory*, vol. 44, no. 6, pp. 1211–1222, 2009.

[19] P. Li, W. Chen, D. Li, R. Yu, and W. Zhang, "Wear analysis of two revolute joints with clearance in multibody systems," *Journal of Computational and Nonlinear Dynamics*, vol. 11, no. 1, Article ID 011009, 2016.

[20] Z. Bai, Y. Zhao, and X. Wang, "Wear analysis of revolute joints with clearance in multibody systems," *Science China Physics, Mechanics and Astronomy*, vol. 56, no. 8, pp. 1581–1590, 2013.

[21] B. Zhao, Z.-N. Zhang, and X.-D. Dai, "Modeling and prediction of wear at revolute clearance joints in flexible multibody systems," *Proceedings of the Institution of Mechanical Engineers, Part C: Journal of Mechanical Engineering Science*, vol. 228, no. 2, pp. 317–329, 2014.

[22] S. Mukras, N. H. Kim, N. A. Mauntler, T. L. Schmitz, and W. G. Sawyer, "Analysis of planar multibody systems with revolute joint wear," *Wear*, vol. 268, no. 5-6, pp. 643–652, 2010.

[23] Z. F. Bai, Y. Zhao, and J. Chen, "Dynamics analysis of planar mechanical system considering revolute clearance joint wear," *Tribology International*, vol. 64, pp. 85–95, 2013.

[24] W. Xiang, S. Yan, and J. Wu, "A comprehensive method for joint wear prediction in planar mechanical systems with clearances considering complex contact conditions," *Science China Technological Sciences*, vol. 58, no. 1, pp. 86–96, 2015.

[25] G. Wang, H. Liu, and P. Deng, "Dynamics analysis of spatial multibody system with spherical joint wear," *Journal of Tribology*, vol. 137, no. 2, Article ID 021605, 2015.

[26] C. C. de Wit and P. Lischinsky, "Adaptive friction compensation with partially known dynamic friction model," *International Journal of Adaptive Control and Signal Processing*, vol. 11, no. 1, pp. 65–80, 1997.

[27] X. Chen, S. Jiang, S. Wang, and Y. Deng, "Dynamics analysis of planar multi-DOF mechanism with multiple revolute clearances and chaos identification of revolute clearance joints," *Multibody System Dynamics*, vol. 47, 2018.